


Article

Optimization of Temperature Sensing with Polymer-Embedded Luminescent Ru(II) Complexes

Nelia Bustamante [†], Guido Ielasi, Maximino Bedoya and Guillermo Orellana * 

Chemical Optosensors and Applied Photochemistry Group (GSOLFA), Department of Organic Chemistry, Faculty of Chemistry, Universidad Complutense de Madrid, E-28040 Madrid, Spain; nbustamante@aenor.es (N.B.); gielasi@ucm.es (G.I.); mabedoya@ucm.es (M.B.)

* Correspondence: orrellana@quim.ucm.es; Tel.: +34-913-944-220

[†] Current address: AENOR, Génova, 6, E-28004 Madrid, Spain.

Received: 29 January 2018; Accepted: 22 February 2018; Published: 26 February 2018

Abstract: Temperature is a key parameter in many fields and luminescence-based temperature sensing is a solution for those applications in which traditional (mechanical, electrical, or IR-based) thermometers struggle. Amongst the indicator dyes for luminescence thermometry, Ru(II) polyazaheteroaromatic complexes are an appealing option to profit from the widespread commercial technologies for oxygen optosensing based on them. Six ruthenium dyes have been studied, engineering their structure for both photostability and highest temperature sensitivity of their luminescence. The most apt Ru(II) complex turned out to be bis(1,10-phenanthroline) (4-chloro-1,10-phenanthroline)ruthenium(II), due to the combination of two strong-field chelating ligands (phen) and a substituent with electron withdrawing effect on a conjugated position of the third ligand (4-Clphen). In order to produce functional sensors, the dye has been best embedded into poly(ethyl cyanoacrylate), due to its low permeability to O₂, high temperature sensitivity of the indicator dye incorporated into this polymer, ease of fabrication, and excellent optical quality. Thermosensitive elements have been fabricated thereof as optical fiber tips for macroscopic applications (water courses monitoring) and thin spots for microscopic uses (temperature measurements in cell culture-on-a-chip). With such dye/polymer combination, temperature sensing based on luminescence lifetime measurements allows 0.05 °C resolution with linear response in the range of interest (0–40 °C).

Keywords: temperature; luminescent sensors; luminescence lifetime; optical fiber; Ru(II) dyes; poly(ethyl cyanoacrylate); water monitoring

1. Introduction

Temperature is one of the most important parameters in industrial process control, environmental monitoring, medicine practice, and biology, to name a few areas [1]. Although measurement of temperature by mechanical or electrical methods is widely established, quantification of this physical magnitude can be sometimes extremely difficult due to hostile media for the operator, restricted accessibility, and/or the presence of strong electromagnetic fields that preclude the use of conventional thermometers. Besides, when studying temperature at the micro- and nanoscale, the latter may lack spatial resolution [2]. Commercially available non-contact IR thermometry may be used under some of those particular situations provided that there is a straight free path between the measuring device and the sample point, and the sample is large enough [3]. When these requirements are not met, fiber-optic sensing offers a convenient alternative. Among the various temperature-dependent optical properties that can be used to develop a temperature *optode* (optical sensor), luminescence thermometry, encompassing fluorescence, and phosphorescence, is probably the most sensitive and

versatile technique [4], as it shows particular advantages. Firstly, it provides unbeatable spatial resolution, down to intracellular temperature sensing [5,6]; it can also be used for imaging temperature gradients [7,8] and it allows for simultaneous monitoring of temperature and other (chemical) parameters [9,10]. Moreover, luminescence lifetime measurements offer the advantages of being immune to the material photodegradation, indicator leaching, excitation source or detector aging, and to fiber-optic bending.

Many papers and patents have been published about the numerous luminescent materials known, the emission of which is strongly dependent on temperature. Examples are inorganic luminescent phosphors, lanthanide-doped bulk materials, quantum dots, biomolecules, organic molecules, lanthanide chelates, and metal complexes [2,11].

In the last two decades, there has been a strong interest in improving molecular oxygen monitoring using optosensor technologies based on luminescence lifetime quenching of Ru(II) complexes or porphyrins [12]. As a consequence, novel fiber-optic devices have already been marketed for environmental, industrial, or clinical measurements with these robust optodes [13]. Temperature sensing with Ru(II) polypyridyls has also been reported [10,14,15]. It has the advantage of profiting from the vast amount of research and development put forward for fiber-optic O₂ measurements with such phosphors. Surprisingly enough, it seems that the only temperature indicators of this class used so far have been those already employed for O₂ sensing [2,7], namely the tris(2,2'-bipyridine)ruthenium(II) [16–19], tris(1,10-phenanthroline)ruthenium(II) [15,20–23], and tris(4,7-diphenyl-1,10-phenanthroline)ruthenium(II) complexes [15,24], with the exception of one particular low-temperature application of bis(terpyridine)ruthenium(II) [25]. However, as we will show, the same photochemical features that confer some Ru(II) dyes a good sensitivity to O₂ [26], make them less sensitive to temperature as well. Moreover, Ru(II) polypyridyls whose luminescence is strongly dependent on temperature, are also the least photostable (see Background section below).

In this paper, we describe how it is possible to design and prepare Ru(II) dyes that are specifically tailored to display a large temperature coefficient for their luminescence intensity and lifetime, while keeping the excellent photostability that characterizes the O₂ indicator complexes. Moreover, selecting an optimum polymer support for the metal chelate is of paramount importance in order to prevent cross-sensitivity to O₂ without slowing down the sensor response. The developed temperature optode provides also a way to correct O₂ (and any other Ru(II)-based) optosensors for the temperature effect by employing the very same instrumentation. The best novel Ru(II) complex has been used here in two different formats, both using a fiberoptic phase shift-based luminometer: (i) as mm-thick polymer monolith onto the optical fiber tips (e.g., for water monitoring applications), and (ii) as μm-thick films into organ-on-a-chip devices, monitored from outside the chip with the optical fibers placed onto the sensitive spots.

Background. In the absence of emission quenchers, the excited state lifetime of luminescent dyes depends on the competition between radiative and non-radiative deactivation processes. In the case of Ru(II) polypyridyl complexes, it has been demonstrated [27–29] that thermal activation can promote the photoexcited electron of the metal dye, located in a luminescent metal-to-ligand charge transfer (³MLCT) manifold of three closely spaced states (Figure 1), to a nearby ³MLCT excited state (so-called “fourth ³MLCT”), and often also to a higher lying non-emissive metal-centered state (³MC). The non-radiative constant corresponding to the thermal activation process follows Arrhenius-type kinetics, so that the temperature dependence of the luminescence lifetime (τ , i.e., the inverse of the excited state deactivation rate constant, k_d) for a Ru(II) complex can be expressed according to Equation (1) [30],

$$\tau = 1/k_d = [A + B \exp(-\Delta E/k_B T)]^{-1} \quad (1)$$

where A represents the temperature-independent term that includes both radiative and non-radiative deactivation constants from the ³MLCT excited state, and B is the pre-exponential factor in the Arrhenius equation. The ΔE parameter stands for the energy gap (if the crossing is a reversible process)

or the activation energy (if it is irreversible) between the $^3\text{MLCT}$ manifold and the thermally accessible excited state, k_B is the Boltzman constant, and T is the absolute temperature.

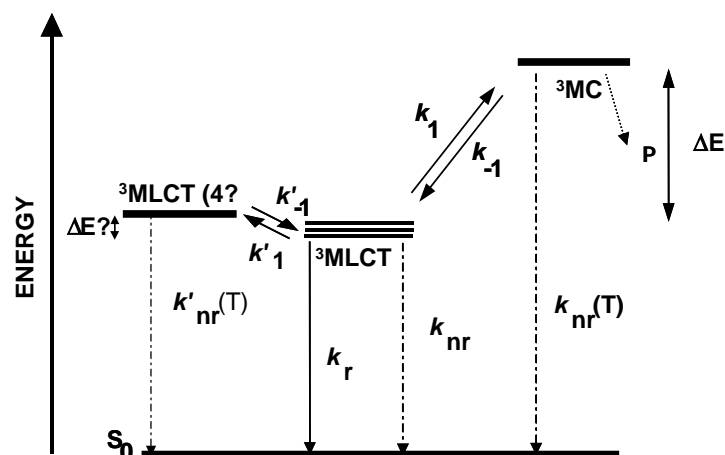


Figure 1. Simplified excited state deactivation diagram for a Ru(II) complex with polyazaheterocyclic chelating ligands. The picture depicts only the emitting and the thermally-activated (dark) excited states.

From Equation (1), it can be inferred that the temperature sensitivity of the luminescent Ru(II) complexes increases with the accessibility to their ^3MC state. However, a very efficient crossing to this excited state leads to photolabile species, due to the anti-bonding nature of σ -type ^3MC states ($e(d^*)$) [31]. The relative energy of the metal-centered level basically depends on the σ -donor features of the chelating ligands (average ligand field strength), while the position of the luminescent $^3\text{MLCT}$ manifold is determined by the energy of the lowest-lying π^* orbital of the ligand set. Therefore, we propose that the synthesis of photostable yet temperature-sensitive Ru(II) indicator dyes should be feasible by selecting appropriate polyazaheterocyclic ligands for engineering heteroleptic (i.e., made of different ligands) metal complexes.

2. Materials and Methods

2.1. Luminescent Dyes

The homoleptic complexes tris(1,10-phenanthroline)ruthenium(II) dichloride, abbreviated $[\text{Ru}(\text{phen})_3]\text{Cl}_2$, tris(2,2'-bipyridine)ruthenium(II) dichloride, abbreviated $[\text{Ru}(\text{bpy})_3]\text{Cl}_2$, and tris(4,7-diphenyl-1,10-phenanthroline)ruthenium(II) dihexafluorophosphate, abbreviated $[\text{Ru}(\text{dpp})_3](\text{PF}_6)_2$, were from Sigma-Aldrich (St. Louis, MO, USA) and were used without further purification. Tris(2,2'-bipyrazine)ruthenium(II) dihexafluorophosphate, abbreviated $[\text{Ru}(\text{bpz})_3](\text{PF}_6)_2$, was synthesized according to standard procedures [32] by refluxing the corresponding commercial ligand (Sigma-Aldrich, St. Louis, MO, USA) (Figure 2) with RuCl_3 trihydrate (Alfa Aesar, Karlsruhe, Germany) in ethylene glycol (+99.5%, Panreac, Castellar del Vallès, Spain), and precipitating the PF_6^- salt by adding a concentrated aqueous solution of NH_4PF_6 (Fluka, Buchs, Switzerland). Commercial $[\text{Ru}(\text{bpy})_3]\text{Cl}_2$ and $[\text{Ru}(\text{phen})_3]\text{Cl}_2$ were metathesized in aqueous solution to their PF_6^- salts by a similar procedure. Preparation of *cis*- $\text{Ru}(\text{phen})_2\text{Cl}_2$ was carried out, as described in the literature [33]. The heterocyclic chelating ligands 4-hydroxy-1,10-phenanthroline (4-OHp) and 4-chloro-1,10-phenanthroline (4-Clp) (Figure 2) were synthesized following the Snyder et al. procedure [34]. $[\text{Ru}(\text{phen})_2(4\text{-OHp})]^{2+}$ and $[\text{Ru}(\text{phen})_2(4\text{-Clp})]^{2+}$ were obtained by refluxing a 10% excess of the corresponding ligand with *cis*- $\text{Ru}(\text{phen})_2\text{Cl}_2$ in 6 mM sodium methoxide/methanol (anhydrous) or ethanol/water (5:1 *v/v*), respectively [35,36]. The crude complexes were purified by flash chromatography on CM-Sephadex[®] (GE Healthcare, Chicago, IL, USA), using an aq. NaCl

gradient as the eluent. Their chemical structure was confirmed by high-field $^1\text{H-NMR}$ spectroscopy and MS-ESI spectrometry [35,36].

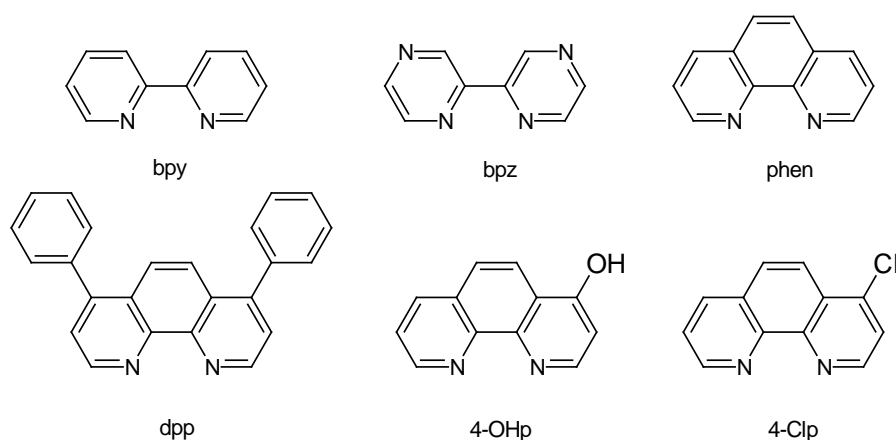


Figure 2. Chemical structure of the chelating ligands used in this work.

2.2. Solvents and Polymer Supports

Propylene carbonate (PC) was from Merck (+99.7%). Methyl methacrylate (MMA, +99%, Merck, Darmstadt, Germany) was distilled under reduced pressure after removing the polymerization inhibitor it contains by washing with aqueous sodium hydroxide (5% *w/v*). Azobis(isobutyro)nitrile (AIBN, +98%, Sigma-Aldrich, St. Louis, MO, USA) was recrystallized from methanol. Ethyl hydroxymethylacrylate (EHMA) was prepared following a reported method [37]. Ethyl 2-cyanoacrylate (“Super-Glue 3[®]”) and two-component epoxy resin (Scotch-Weld DP-100) were from Loctite (Düsseldorf, Germany) and 3M (Maplewood, MN, USA), respectively. Tetraethoxysilane (98%) was from Merck (Darmstadt, Germany).

2.3. Spectroscopic Measurements

UV-VIS spectra were collected in a Cary-3Bio spectrophotometer (Varian, Palo Alto, CA, USA). Steady-state emission spectra in solution were recorded at 25 °C in a Perkin-Elmer LS50-B spectrofluorometer. Quartz cells for fluorescence (10 × 10 mm², Hellma, Müllheim, Germany) have been employed for all of the spectroscopic determinations. Time-drive luminescence measurements were performed with a portable fiber-optic spectrometer (Guided Wave model 260), fitted with colored glass band-pass and long-pass filters (Oriol-Newport, Irvine, CA, USA) centered at 400 and 570 nm, respectively. The luminescence quantum yield of [Ru(phen)₂(4-Clp)]Cl₂ in deoxygenated water was measured by the Parker and Rees method [38], using [Ru(bpy)₃]Cl₂ as reference dye ($\Phi_{\text{em}} = 0.063$ [39]).

2.4. Luminescence Lifetimes

Emission decay measurements in solution were performed with a single photon timing spectrometer (SPT, Edinburgh Instruments FLS-980, Livingston, UK) equipped with a 450 nm LED head (Nanoled 450L, Horiba, Kyoto, Japan) ns-pulsed at 20 or 40 kHz as the excitation source (through a 467 nm interference filter) and a red-sensitive Hamamatsu R-955 photomultiplier cooled at −20 °C. Solutions of the ruthenium complexes in PC (7–16 μM) were deoxygenated with argon (>99.99%, Praxair, Madrid, Spain), sparging them for at least 30 min before collecting the emission decays. The luminescence lifetimes of the sensor tip were also measured as a function of temperature with the SPT spectrometer. The cuvette sample holder of the FLS-980 was replaced by a homemade fiber-optic adapter to which a (randomly) bifurcated silica waveguide bundle was connected (FiberGuide, Township, NJ, USA, 6.5 and 4.5 mm diameter at the common end and at each branch, respectively). The emission decays were fitted to a single exponential function (solutions) or to the minimum number

of summed exponentials (doped polymers) to achieve a reduced χ^2 value lower than 1.1 using the Edinburgh Instruments proprietary software based on non-linear least squares fitting. Caution must be exercised with multi-exponential decay functions because they might not correspond to the presence of a discrete number of luminescent species, but rather to a plurality of luminophore populations of different widths, as shown by the Edinburgh Instruments (Livingston, UK) advanced Fluorescence Analysis Software Technology (FAST).

2.5. Phase-Sensitive Luminescence Measurements

Phase-sensitive monitoring was carried out with a field-deployable fiberoptic phase-sensitive luminometer developed in our research group. The instrument is able to determine simultaneously up to four target parameters (e.g., temperature, O₂, moisture, CO₂), or a single parameter in different locations, using common electronic and optoelectronic components, but specific Ru(II) polypyridyls immobilized in tailored polymer supports. The system is equipped with four 470 nm LEDs (9600 mcd, RS Amidata, Madrid, Spain) as excitation light sources, digitally modulated at 39, 78, or 156 KHz (user selectable). The optical module contains a 450 nm CS5-60 colored band-pass filter (100 nm FWHM) (Kopp Glass, Pittsburgh, PA, USA) in the excitation channel, a 503 nm dichroic filter (Edmund Optics, York, UK), and a 570 nm long-pass filter (CS2-73, Kopp), plus a plano-convex lens with 4 mm effective focal length (Edmund) in the emission channel. The excitation light is focused onto a 1000 μm multimode plastic optical fiber (Mitsubishi Cable, Tokyo, Japan) fitted with a SMA connector (Ratioplast Optoelectronics, Lübbecke, Germany). The luminescence from the four sensitive terminals is monitored with an H11901-01 compact photomultiplier (Hamamatsu Photonics, Hamamatsu, Japan). The reference signal is obtained directly from the excitation blue LEDs with one Hamamatsu S5821-03 photodiode per optical channel. The instrument configuration and data are stored in the unit and can be transferred at any time to and from a laptop computer via the RS232 or USB ports, using our Windows-based software.

The measured phase shift (ϕ) and the luminescence lifetime (τ), for a particular modulation frequency of the excitation light source (f), are related through the well-known Equation (2) [40]:

$$\tan \phi = 2\pi f\tau \quad (2)$$

If the emission decay is perfectly exponential (e.g., in isotropic solutions of the luminophore), the observed ϕ can be used to determine the τ instead of the single photon timing technique. However, if the excited state decay is an ensemble of luminophore molecules in different microenvironments, the value of τ calculated from ϕ is an averaged one, which also depends on the modulation frequency and is not always coincident with the pre-exponentially weighted emission lifetime determined from SPT (see Section 3.4) [41]. All spectroscopic, emission lifetime, and luminescence phase shift measurements have been performed on fully cured (>5 days) polymer materials (see below) unless otherwise stated.

Temperature sensing with the phase shift-based luminometer was carried out in two ways: on the one hand, the temperature-sensitive polymer layers (see below) were attached to the optical fiber tips, for realizing environmental/industrial monitoring instrumentation. On the other hand, sensitive layers were deposited into organ-on-a-chip devices for monitoring the internal temperature from the outside with the fiberoptic luminometer.

2.6. Temperature Control

For the macroscopic monolithic sensor tips, temperature was kept within ± 0.25 °C with a digital water bath/circulator (mod. 9110, Polyscience, Niles, IL, USA). When working at temperatures below 0 °C, a water/ethylene glycol (1:1 *v/v*) mixture was employed as cryogenic fluid. For testing the microscopic temperature-sensitive films, temperature was controlled with a heating plate (IKA[®])

RCT basic, Staufen, Germany) and monitored with a commercially available thermistor (LM335, Texas Instruments, Dallas, TX, USA).

2.7. Fabrication of the Sensor Tips

A copolymer of EHMA and MMA doped with the temperature indicator dye was prepared by dissolving 0.23 mg of $[\text{Ru}(\text{phen})_2(4\text{-Clp})]\text{Cl}_2$ in 0.1 mL of EHMA, and mixing the solution with 3 mL of MMA containing 0.23 mg of AIBN. Round-bottomed glass tubes ($50 \times 6 \text{ mm}^2$, 5 mm i.d.) were filled with ca. 0.5 mL of the mixture, sonicated for 10 min and heated at $60 \text{ }^\circ\text{C}$ for 72 h. A piece of ca. 3 mm from the bottom of the Ru-doped polymer matrix was cut after drawing the cured material out of the mold, polishing several times with sand paper of increasingly fine grain the flat side to be in contact with the optical fiber.

Sol-gel glasses were produced from a mixture of ethanol (1.2 mL), deionized water (0.56 mL), and tetraethoxysilane (1 mL), after increasing the drying temperature up to $700 \text{ }^\circ\text{C}$ with a laboratory oven ($0.5 \text{ }^\circ\text{C}/\text{min}$). After formation of the monolith, differential absorbance measurements of the supernatant showed that 4 mol of the ruthenium complex, dissolved in ethanol, was incorporated into 300 mg of this porous matrix (72 h contact time).

Sensor tips prepared from a commercial epoxy resin (see above) were fabricated by dissolving ca. 0.2 mg of the dye in 1.5 mL of 2-butanone (99%, Merck, Darmstadt, Germany, DE), and adding the same amount of the hardener and the epoxy components to this solution. Borosilicate round-bottomed glass tubes were filled with this mixture, which was allowed to polymerize at room temperature for 72 h. The Ru-doped monoliths were cut and polished, as described before for EHMA-MMA copolymer.

Poly(ethyl cyanoacrylate) (PCA) monoliths containing the temperature indicator complex were prepared by filling the above mentioned borosilicate molds with ca. 500 μL solution of the Ru(II) complex in the monomer (0.20–0.35 mg in 4 mL). Due to the relatively large solution volume, CA polymerizes slowly, so that changes in the luminescence from the dyed material were observed over the first five days (see Results and Discussion section). Therefore, all of the monoliths were allowed to cure for at least five days to obtain sensors showing a stable response. After this period, the borosilicate tube was broken to extract the solid matrix. Then it was cut to ca. 1.5 mm and thoroughly polished according to the procedure described above to yield 1-mm high domed monoliths. The latter are placed in direct contact with the distal end of the optical fiber, mounted in home-made stainless-steel ferrules after covering the outermost part of the monolith with aluminum foil to eliminate the interference of the external light on the luminescence from the dyed polymer (Figure S1, Supplementary Materials). The application of a black painting overcoat was also successfully tested.

2.8. Temperature-Sensing Film in Microfluidic Devices

Organ-on-a-Chip devices were kindly provided by Micronit Microtechnologies (Enschede, The Netherlands) (<https://www.micronit.com/products/organ-on-a-chip.html>). These chips consist of three layers: a thin glass membrane-carrier sandwiched between two glass slides equipped with integrated gaskets (Figure S2a, Supplementary Materials). The gaskets are made of a perfluorinated elastomer, and are fabricated by means of a dispensing computer numerical control machine. The flow chambers are created by mechanically compressing the three layers using the dedicated (but customizable) Micronit Fluidic Connect Pro clamp (Figure S2c, Supplementary Materials). This sealing strategy yields flow channels without the need of thermal or chemical processes, and allows for re-opening the chips at any time just by opening the clamp. Temperature-sensitive $[\text{Ru}(\text{phen})_2(4\text{-Clp})]^{2+}$ -dyed PCA films, with a thickness lower than 100 μm to match the size of the channel, are deposited in the internal part of the top glass slide, as described below. Sheets of polyimide tape (Kapton[®], DuPont) of 50 μm thickness were cut into 15 mm \times 45 mm pieces with three holes (4 mm dia.) along the long axis, using a cutting plotter (Graphtec CE6000-60, Irvine, CA, USA). The patterned tape sections were then transferred onto the glass slide and used as a deposition mask. Solutions of the dye (67 μM) in the pure monomer were knife-coated onto the Kapton[®] tape-coated glass, and the tape

was immediately removed leaving behind three round-shaped spots of dyed solution. In some cases, the latter were covered with a piece of 15 μm -thick aluminum foil, which remained glued onto the dyed cyanoacrylate film. The luminescent spots were allowed to cure for 24 h and fiber-optic interrogation was always made from the uncovered side of the polymer film (Figure S2b, Supplementary Materials).

3. Results and Discussion

3.1. Indicator Dye Selection

The development of a novel indicator-based luminescent sensor involves an initial stage of selecting the optimum dye for a suitable analyte detection. To that aim, six Ru(II) complexes containing different chelating ligands, namely $[\text{Ru}(\text{bpy})_3](\text{PF}_6)_2$, $[\text{Ru}(\text{bpz})_3](\text{PF}_6)_2$, $[\text{Ru}(\text{phen})_3](\text{PF}_6)_2$, $[\text{Ru}(\text{dpp})_3]\text{Cl}_2$, $[\text{Ru}(\text{phen})_2(4\text{-OHp})](\text{PF}_6)_2$, and $[\text{Ru}(\text{phen})_2(4\text{-Clp})]\text{Cl}_2$ (Scheme II), were chosen. The electronic features of the selected coordination ligands span from the significant σ -donor ability of 4-OHp to the highly π -accepting bpz. The intermediate σ -donating properties of the other chelating ligands decrease in the sequence $\text{bpy} > \text{phen} > \text{dip} > 4\text{-Clp}$, while their π -accepting character increases from bpy to 4-Clp. The luminescence decay profile of these complexes was recorded as a function of temperature to establish the influence of the structure and number of specific polypyridyl ligands on the $^3\text{MLCT}$ excited state deactivation kinetics of the corresponding metal complexes. The emission decays in propylene carbonate (PC) could be fitted to single-exponential functions, except that shown by the $[\text{Ru}(\text{bpz})_3]^{2+}$ complex for which a biexponential fit had to be used at temperatures above 35 $^\circ\text{C}$. Moreover, an exponential fit could not be recovered after cooling down the solution containing this dye, pointing out to an irreversible thermal transformation of the luminescent indicator in the organic solvent. The known instability of $[\text{Ru}(\text{bpz})_3]^{2+}$ is attributable to the very weak σ -donation properties of the bipyrazine when compared to either bipyridine or phenanthroline ligands [42,43]. The weak ligand field strength of bpz and related ligands approaches the $^3\text{MLCT}$ and the (dissociative) ^3MC excited states, with deleterious results for the luminescent probe design.

Fitting the experimental emission lifetimes obtained at different temperatures (Figure 3) to Equation (1) allows determination of the parameters of the fit (Table 1).

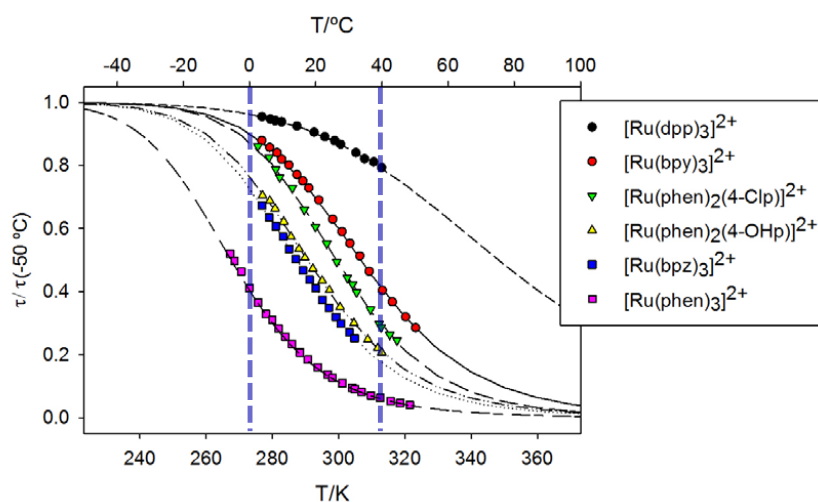


Figure 3. Luminescence lifetimes (normalized at 223 K) as a function of temperature of the Ru(II) complexes in deoxygenated propylene carbonate solution (PC-11 N aq HCl 10:1 v/v for the hydroxylated complex). The black lines stand for the best computer fit (Sigma Plot 11.0) of the experimental data to Equation (1), assuming contribution of only one thermally activated pathway. From top to bottom: (—●—) $[\text{Ru}(\text{dpp})_3]^{2+}$; (—●—) $[\text{Ru}(\text{bpy})_3]^{2+}$; (—▼—) $[\text{Ru}(\text{phen})_2(4\text{-Clp})]^{2+}$; (—▲—) $[\text{Ru}(\text{phen})_2(4\text{-OHp})]^{2+}$; (—■—) $[\text{Ru}(\text{bpz})_3]^{2+}$; (—■—) $[\text{Ru}(\text{phen})_3]^{2+}$. The blue vertical dashed lines highlight the range 0–40 $^\circ\text{C}$ range of interest for the sought applications.

Table 1. Kinetic parameters for the ³MLCT excited state deactivation of the investigated Ru(II) complexes in deoxygenated propylene carbonate, obtained from fitting the experimental emission lifetime data as a function of temperature to Equation (1) (see text).

| Complex | $A \times 10^3$ /s ⁻¹ | $B \times 10^{11}$ /s ⁻¹ | ΔE /cm ⁻¹ | r | $\tau/\mu\text{s}^a$ | $k_t \times 10^{-5}$ /s ⁻¹ a,b | $\eta_t^{a,c}$ |
|---|-------------------------------------|--|---------------------------------|--------|----------------------|--|----------------|
| [Ru(phen) ₃] ²⁺ | 235 ± 5 | 446 ± 89 | 3546 ± 23 | 0.9998 | 0.53 ± 0.01 | 1.6 | 0.08 |
| [Ru(dpp) ₃] ²⁺ | 146 ± 1 | 0.2 ± 0.1 | 2861 ± 162 | 0.9993 | 6.0 ± 0.1 | 0.2 | 0.14 |
| [Ru(bpy) ₃] ²⁺ | 656 ± 8 | 481 ± 219 | 3858 ± 100 | 0.9996 | 0.96 ± 0.02 | 3.9 | 0.37 |
| [Ru(phen) ₂ (4-Clp)] ²⁺ | 236 ± 4 | 1500 ± 937 | 4215 ± 134 | 0.9995 | 2.22 ± 0.04 | 2.2 | 0.48 |
| [Ru(phen) ₂ (4-OHp)] ²⁺ d | 276 ± 10 | 347 ± 228 | 3764 ± 141 | 0.9995 | 1.40 ± 0.03 | 4.4 | 0.62 |
| [Ru(bpz) ₃] ²⁺ | 388 ± 10 | 753 ± 344 | 3808 ± 96 | 0.9998 | 0.87 ± 0.02 | 7.8 | 0.67 |

^a At 298 K; ^b $k_t = B \exp(-\Delta E/kT)$; ^c Efficiency of the thermally-activated promotion from the ³MLCT excited state to the ³MC: $\eta_t = k_t / (k_r + k_{nr} + k_t) = k_t \tau$ (see Figure 1); ^d In propylene carbonate–aq. HCl (11 N), 10:1 v/v.

Due to the significant covariance observed between the B and ΔE parameters of the fit, they cannot be analyzed separately: only their order of magnitude and the rate constant of the temperature-activated crossing ($k_t = B \exp(-\Delta E/kT)$) are meaningful quantities [44]. In this way, $B > 10^{12} \text{ s}^{-1}$ and $\Delta E > 3000 \text{ cm}^{-1}$ values (at 298 K) have been attributed to thermal population and decay via the ³MC excited state, whereas $B < 10^8 \text{ s}^{-1}$ and $\Delta E < 800 \text{ cm}^{-1}$ indicate a non-radiative deactivation via the higher-lying (fourth) ³MLCT state [45]. Taking these values into account, the collected data for the Ru(II) luminophores investigated in this work (Table 1) indicate the predominance of the former deactivation pathway in all cases. The long emission lifetime of the [Ru(dpp)₃]²⁺ dye, together with the low efficiency of its thermally-activated deactivation process (η_t), probably mean that the observed decrease of its luminescence upon increasing temperature is due to both decay pathways. This fact would explain the intermediate values of B and ΔE obtained for this dye. The conjugated aromatic structure of dpp increases its π -acceptor features when compared to the unsubstituted phen ligand, leading to stabilization of the metal complex ³MLCT excited state with respect to its ligand-field ³MC level and, therefore, displays longer emission lifetimes and much lower temperature sensitivity. Nevertheless, [Ru(bpy)₃]²⁺ and [Ru(phen)₃]²⁺ are the ruthenium complexes most used in the literature for temperature optosensing, probably taking advantage of the vast amount of information about their luminescent features put forward for fiber-optic O₂ measurements with these dyes [15]. Interestingly, [Ru(phen)₃]²⁺ is the most sensitive amongst the investigated dyes in the –30 to +20 °C temperature range. However, above 20 °C its luminescence is appreciably quenched so that, at 25 °C, the efficiency of thermally activated promotion from the ³MLCT excited state is the lowest amongst the values obtained in this study.

The photoexcited [Ru(bpz)₃]²⁺ is the most sensitive complex in the temperature range of interest due to its high η_t value. Unfortunately, this efficient promotion to the dark ³MC state leads to fast photodecomposition, making it unsuitable for luminescent temperature sensing. The luminescence lifetime of [Ru(phen)₂(4-OHp)]²⁺ also shows a strong dependence with temperature but only in acidic PC (Table 1) due to the almost complete loss of its luminescence when deprotonated. The high η_t value found for this indicator (Table 1), close to that of [Ru(bpz)₃]²⁺, also leads to a high photolability. Similarly to the pyrazine moieties (see above), but in a lower degree, the electron withdrawing effect of the chlorine atom on the phenanthroline moiety leads to stabilization of the ³MLCT excited state in [Ru(phen)₂(4-Clp)]Cl₂. However, this complex also contains two unsubstituted phen ligands coordinated to the metal core, the strong σ -donation of which results in destabilization of its ³MC level (strong ligand field). Therefore, this metal complex shows good photostability as a consequence of its high ΔE value (4215 cm⁻¹). At the same time, its very large pre-exponential factor ($1.5 \times 10^{14} \text{ s}^{-1}$) leads to significant temperature dependence, making it the best choice for a lifetime-based luminescent temperature indicator dye to be used both in the 0 to 50 °C range (water monitoring applications) [46], and the 25 to 40 °C range (cell culture applications) [47,48].

3.2. Photophysical Characterization of $[\text{Ru}(\text{Phen})_2(4\text{-Clp})]^{2+}$ in Solution

The absorption and emission maxima of $[\text{Ru}(\text{phen})_2(4\text{-Clp})]^{2+}$ in different organic solvents and in water, together with its luminescence lifetimes in air-equilibrated and deoxygenated solutions, are summarized in Table 2. The selected organic solvents try to simulate the environment around the indicator dye in the best polymer matrix (see Section 3.3). The absorption spectra show intense UV bands corresponding to intraligand (IL) $\pi \rightarrow \pi^*$ transitions and a broad band, with two maxima in the visible region, assigned to a metal-to-ligand charge transfer transition ($d \rightarrow \pi^*$) [31]. No significant solvent effect has been observed either on the maxima or on the intensity of the absorption bands within the relatively polar solvents used in this work. This complex also displays, as expected, an unstructured emission band centered at 610–619 nm, depending on the solvent polarity and viscosity. The differences found in the emission lifetime as a function of the solvent can be explained in terms of the corresponding oxygen solubility (higher in organic solvents), solvent viscosity, and energy transfer to the solvent O–H oscillators.

Table 2. Spectroscopic features and emission lifetimes of $[\text{Ru}(\text{phen})_2(4\text{-Clp})]^{2+}$ in solution at 25.0 °C.

| Solvent | $\Delta\lambda_{\text{max}}^{\text{abs}}/\text{nm}$ ($\epsilon/\text{M}^{-1}\text{cm}^{-1}$) ^a | $\Delta\lambda_{\text{max}}^{\text{em}}/\text{nm}$ ^b | $\tau_{\text{Air}}/\mu\text{s}$ ^c | $\tau_{\text{Ar}}/\mu\text{s}$ ^c |
|---------------------|--|---|--|---|
| water | 224 (59,500), 262 (83,000), 425 (13,900), 445 (14,100) | 610 | 0.82 | 1.49 ^d |
| propylene carbonate | 224, 262, 425, 445 | 619 | 0.51 | 2.22 |
| acetonitrile | 224, 262, 425, 445 | 612 | 0.24 | 1.90 |
| butyronitrile | 224, 262, 425, 445 | 610 | 0.34 | 1.63 |

^a Uncertainty ± 1 nm; the uncertainty for ϵ is $\pm 10\%$; ^b Uncorrected for the instrumental response; uncertainty ± 2 nm; ^c Uncertainty 2%; ^d Luminescence quantum yield (Φ_{em}) under these conditions: (0.12 ± 0.01) .

3.3. Polymer Sensor Tip Development

After photophysical characterization of the selected Ru(II) dye in solution, four polymeric matrices were tested in order to find the best solid support for the dye immobilization without altering its temperature-sensing features. A facile manufacturing of the dye-doped polymer material, together with a good thermal conductivity and low oxygen permeability were the main searched characteristics for the temperature sensor matrix. The investigated polymers were a sol-gel material, an epoxy resin, poly(ethyl cyanoacrylate) (PCA), and a copolymer of an hydroxylated acrylate monomer (EHMA) and MMA (see Experimental section). The scarce solubility of the Ru(II) complex in pure MMA led us to copolymerize this monomer with its hydroxylated derivative where the dye was soluble in.

The temperature sensitivity of the dye entrapped in the polymeric supports, in terms of the relative change in the luminescence intensity displayed by the manufactured sensor tip when temperature was dropped from 40 to 0 °C, has been summarized in Table 3. The intensity change for other temperatures is shown in Figure S3 (Supplementary Materials).

Table 3. Temperature sensitivity of the luminescence of $[\text{Ru}(\text{phen})_2(4\text{-Clp})]^{2+}$ immobilized into different polymers.

| Polymer support ^a | PCA | EPOXY | SOL-GEL | p(EHMA-MMA) |
|------------------------------|-----|-------|---------|-------------|
| I_0/I_{40} ^b | 3.6 | 3.3 | 2.2 | 1.8 |

^a PCA: poly(ethyl cyanoacrylate). See Experimental section for details on the sensor materials; ^b Relative emission intensity at 0.0 and 40.0 °C ($\lambda_{\text{em}} = 590$ nm).

Supports containing hydroxyl groups in their structure, such as the sol-gel and p(EHMA-MMA), showed a lower temperature sensitivity, probably due to competitive deactivation of the luminophore via energy transfer to the surrounding O–H oscillators. Moreover, the sensor tip manufactured with the epoxy resin displayed a slower and unstable response to temperature changes, owing to a lower thermal conductivity. On the contrary, luminescently-doped polycyanoacrylate monoliths showed a fast and

stable response (Figure 4), allowing, at the same time, fabrication of readily-made reproducible sensor tips.

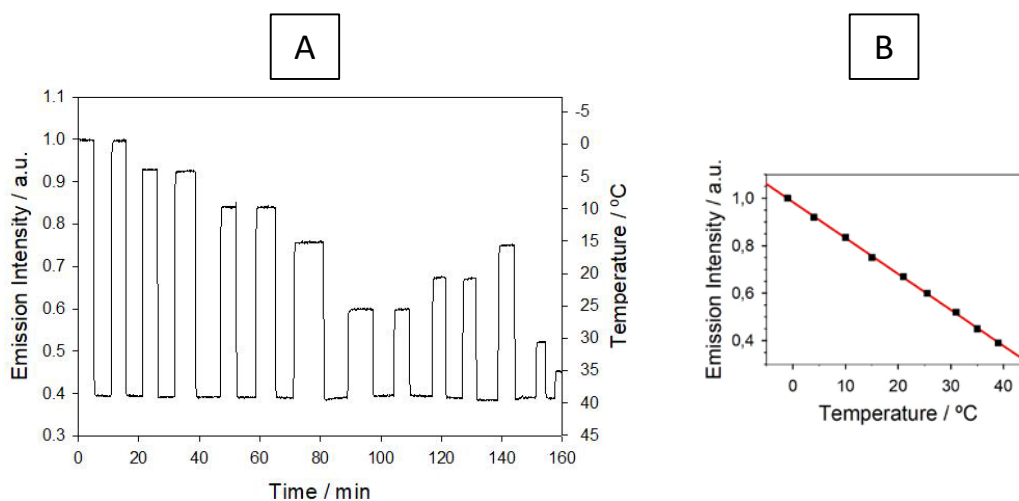


Figure 4. Response of the luminescent temperature sensor containing $[\text{Ru}(\text{phen})_2(4\text{-Clp})]^{2+}$ immobilized into poly(ethyl cyanoacrylate). (A) Real-time response; (B) Calibration plot.

3.4. Photophysical Characterization of the Dye Entrapped into a Poly(Cyanoacrylate) Matrix

Different authors have studied the effect of the polymer support on the photophysical properties of Ru(II) complexes entrapped into rigid matrices. Thus, it has been demonstrated the inhibition of the emission decay through the ^3MC pathway for photoexcited $\text{Ru}(\text{bpy})_3^{2+}$ (and related complexes) immobilized in cellulose acetate [43], zeolites [49], or metal-organic frameworks (MOFs) [50,51], so that its small temperature dependence in the region of interest is then controlled by the additional (fourth) MLCT state. This effect is due to the anti-bonding nature of the excited state ^3MC , because its population is expected to lead to the elongation of the Ru-N bonds that is inhibited in the rigid medium.

We have monitored the changes of the luminescence spectrum of $[\text{Ru}(\text{phen})_2(4\text{-Clp})]^{2+}$ dissolved in the cyanoacrylate monomer during its polymerization. The metal complex displayed a blue shift of its emission band as the monomer became harder (during the first three days, Figure 5). The emitting $^3\text{MLCT}$ cannot be stabilized by solvent reorganization in the solid matrix (rigidochromism), and, therefore, the radiative deactivation takes place from a more energetic excited state leading to the emission blue shift. The luminophore also undergoes a strong enhancement of its luminescence intensity (Figure 5), largely due to the less accessibility of the oxygen to the indicator, which decreases the deactivation pathway that is caused by this effective quencher. The observed changes in the intensity and maximum emission wavelength of the dye dissolved in the monomer also allow for a continuous monitoring of the polymerization process to assess its progress.

Table 4 lists the emission lifetimes obtained from the analysis of the luminescence decay kinetics of the $[\text{Ru}(\text{phen})_2(4\text{-Clp})]/\text{PCA}$ sensor tip. Under the two evaluated temperatures (0.0 and 40.0 °C), the emission decays could only be fitted correctly to 3-exponential functions. Several environments for the dye into the solid matrix are the origin of the different lifetimes found: the longest one is associated to very diluted ruthenium complexes entrapped in the rigid polymer medium, while the shortest one corresponds to aggregated dye molecules dwelling in other regions of the polymer monolith. The bright aggregates undergo nonetheless self-quenching of their emission lifetime, as it has been shown by luminescence lifetime imaging microscopy in O_2 -sensitive polymer layers that are also manufactured with Ru(II) complexes [52]. Actually, the situation is probably more complex and the number of luminophores in different microenvironments of the polymer matrix is expected to be higher than just three. Once the 3-exponential function provides an excellent fit, we do not try a larger

number of exponential terms. Intermediate lifetimes correspond to populations of Ru(II) dye molecules separated by various distances or surrounded by different domains generated by the PCA chains.

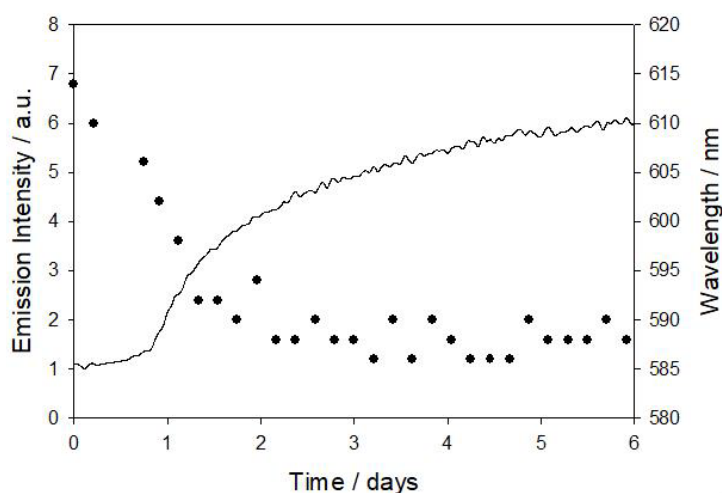


Figure 5. Continuous monitoring of the luminescence intensity (solid line) and maximum emission wavelength (full circles) of the $[\text{Ru}(\text{phen})_2(4\text{-Clp})]^{2+}$ complex dissolved in ethyl cyanoacrylate during polymerization at room temperature.

Table 4. Luminescence lifetimes of $[\text{Ru}(\text{phen})_2(4\text{-Clp})]^{2+}$ in solution and immobilized into the poly(ethyl cyanoacrylate) matrix. The emission decays of the indicator dye have been fitted to the function $I(t) = A_1e^{-t_1/\tau} + A_2e^{-t_2/\tau} + A_3e^{-t_3/\tau}$.

| $T/^\circ\text{C}$ | $\Delta\tau_{\text{PC}}/\mu\text{s}$ ^a | $\tau_1/\mu\text{s}$ (α_1) ^b | $\Delta\tau_2/\mu\text{s}$ (α_2) ^b | $\Delta\tau_3/\mu\text{s}$ (α_3) ^b | τ_M ^c | $\Delta\tau_\phi$ ^d |
|--------------------|---|--|--|--|-----------------------|--------------------------------|
| 0.0 | 3.71 | 5.78 (0.44) | 3.03 (0.36) | 1.27 (0.20) | 3.89 | 3.51 |
| 40.0 | 1.23 | 3.35 (0.30) | 1.19 (0.45) | 0.18 (0.25) | 1.59 | 2.08 |

^a Lifetime in deoxygenated propylene carbonate (PC) solution; ^b The α values represent the relative pre-exponential term ($\alpha_i = A_i / \sum_i A_i$); ^c Pre-exponentially weighted emission lifetime $\tau_M = \sum_i \alpha_i \tau_i$; ^d Average emission lifetime determined from the experimental phase shift (ϕ at $f = 78$ KHz): $\tau_\phi = \tan \phi / 2\pi f$ [41].

3.5. Temperature Measurements Based on the Luminescence Lifetime of the Polymer Material

Macroscopic Temperature-Sensitive Optical Fiber Sensor. After evaluating the temperature optode response by steady-state emission measurements, the optical sensor was evaluated with a fiber-optic phase-sensitive luminometer. To that end, the sensor tips were coated with aluminum foil for protection against the income of external light to the detector, and placed at the end of a single optical fiber (Figure S1). The sensitive terminal was introduced in a temperature-controlled water bath and the emission phase shift, as generated by the luminophore lifetime was continuously recorded (Figure 6). This emission lifetime decreases linearly with temperature in the tested range ($r = 0.99987$), simplifying the optode calibration. A continuous monitoring of the emission intensity was simultaneously carried out thanks to the value of the amplitude of the modulated luminescence waveform provided by the instrument. Intensity values confirm the dye photostability during the measurements.

The optimal modulation frequency of the blue light source (78 kHz) was chosen to provide the maximum difference (14.3°) between the phase angles that were measured at 0 and 40 °C. This temperature range is the most useful for water courses monitoring, the sought application for our luminescent sensor. The apparent small discrepancy between the emission lifetimes of $\text{Ru}(\text{phen})_2(4\text{-Clp})^{2+}$ embedded in PCA calculated from the observed phase shift (τ_ϕ , Figure 6) and those calculated from the multiexponential decay of the luminescence (τ_M , Table 4) is simply due to the different weight of the short and long components (τ_i) in the τ_M calculation and in the overall phase shift. While the former depends on $\alpha_i \tau_i$, the latter rather depends on the modulation frequency,

according to $\alpha_i \tau_i / [1 + (2\pi f)^2 \tau_i^2]$ [41] (pp. 191–192). Therefore, higher modulation frequencies yield shorter τ_ϕ values due to the heavier contribution of the shorter-lived components.

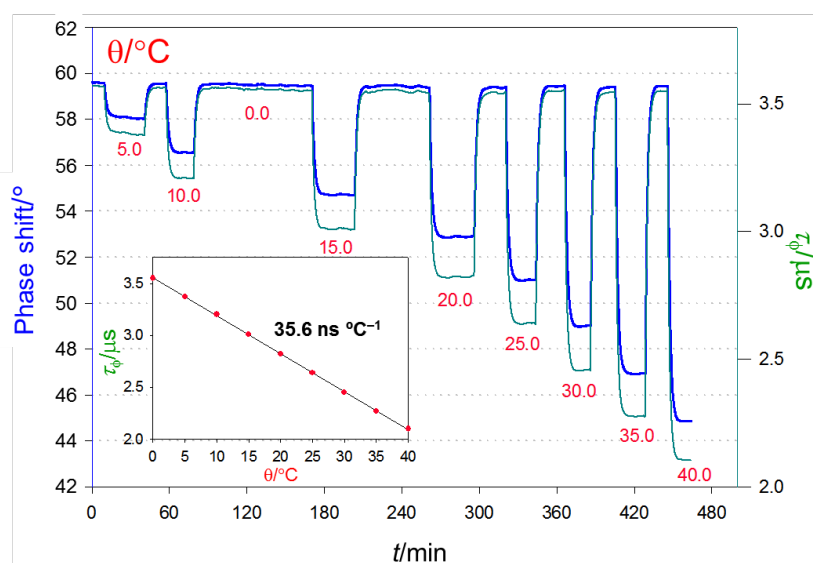


Figure 6. Temperature response of the $\text{Ru}(\text{phen})_2(4\text{-Clp})^{2+}$ -doped poly(ethyl cyanoacrylate) luminescent optode fabricated with an initial concentration of dye in ethyl cyanoacrylate of $29 \mu\text{M}$. The thick blue line represents the experimental raw data (phase shift) measured with the fiber-optic luminometer (excitation LED modulation $f = 78 \text{ KHz}$). The corresponding emission lifetime (thin green line and inset), i.e., the experimental (average) value obtained from the phase shift angle ($\tau_\phi = \tan \phi / 2\pi f$) displays a linear response in the 0 to $40 \text{ }^\circ\text{C}$ range ($r = 0.99987$), with a slope of $35.6 \text{ ns } ^\circ\text{C}^{-1}$.

The effect of the dye loading in the polymer was also investigated. We found a modest 7% increase of ϕ ($0 \text{ }^\circ\text{C}$) in going from an initial concentration of $\text{Ru}(\text{phen})_2(4\text{-Clp})^{2+}$ in ethyl cyanoacrylate of 29 to $67 \mu\text{M}$, accompanied by a 15% decrease of ϕ ($40 \text{ }^\circ\text{C}$); higher levels of doping (up to $114 \mu\text{M}$) lead to negligible further increase of ϕ ($0 \text{ }^\circ\text{C}$), while significantly increasing ϕ ($40 \text{ }^\circ\text{C}$). Those variations translate into phase shift excursions in the 0 – $40 \text{ }^\circ\text{C}$ range of 14.3° at $29 \mu\text{M}$, to 22.6° at $67 \mu\text{M}$. More concentrated initial solutions actually yield smaller excursions of ϕ probably due to larger populations of aggregated dye species and the self-quenching of the photoexcited dye lifetime they undergo (see Section 3.4).

The response time of the temperature luminescent sensor is determined by the calibrated thermostatic circulator change rate. Nevertheless, instantaneous transfer of the fiber-optic sensor tip from an ice-water bath at $0 \text{ }^\circ\text{C}$ to the thermostatic bath at $40 \text{ }^\circ\text{C}$ led to response times on the order of 20 s ($t_{90\%}$). The optode response can be accelerated using thinner PCA/dye monoliths attached to the optical fiber at the expense of a slightly lower sensitivity in the investigated temperature range.

The optode resolution (R), calculated from the calibration slope (s) and the standard deviation, σ_{n-1} , for the worst signal-to-noise ratio (measured at $40.0 \text{ }^\circ\text{C}$), was found to be $0.05 \text{ }^\circ\text{C}$ under the optimized conditions ($R = 3\sigma_{n-1}/s$, $n = 20$). The sensor tip reproducibility and its response repeatability were better than 2% and 1%, respectively, also evaluated from the relative standard deviation of the temperature measurements.

The effect of dissolved molecular oxygen, a well-known efficient quencher of $\text{Ru}(\text{II})$ luminophores (see above), on the response of the optode was also studied (Figure S4, Supplementary Materials). No significant changes were observed when dipping the sensor tip into air equilibrated or fully deoxygenated solutions at identical temperature due to the low oxygen permeability of the selected polymer (PCA). Obviously, any influence of O_2 is suppressed for the aluminum foil-covered polymer monoliths.

Microscopic Temperature-Sensitive Films inside Organ-on-a-Chip Devices. Finally, the optimized sensor was tested for temperature monitoring into organ-on-a-chip devices. The dyed polymer was deposited as thin spots and the chips were subjected to temperature variations from ca. 27 to 52 °C (Figure 7).

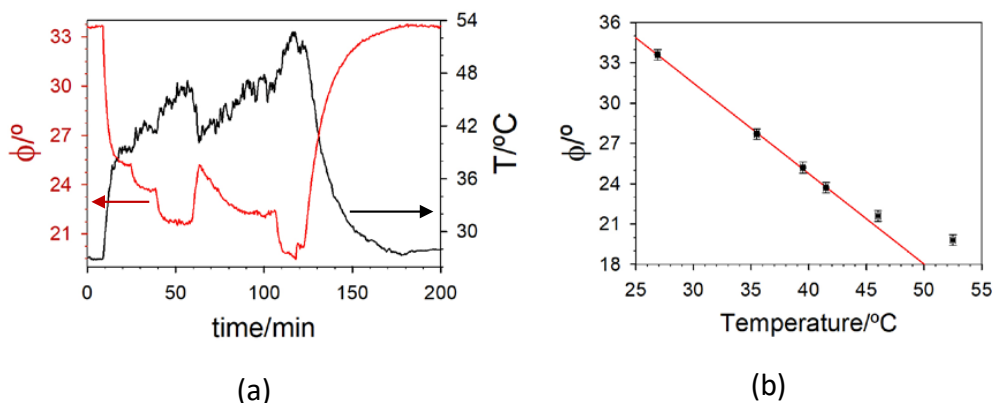


Figure 7. (a) Example of the fiber optic luminescence-based temperature sensor response (red line). The temperature was varied with a heating plate (IKA RCT basic) and monitored with a commercially available thermistor (LM335, Texas Instrument, black line); (b) Phase-shift response with temperature. The red line is the linear fit of the experimental data between 26.9 and 41.5 °C (parameters of the best fit $\phi/^{\circ} = A + b T/^{\circ}C$: $A = (51.7 \pm 0.3)^{\circ}$; $b = (-0.674 \pm 0.009)^{\circ}C^{-1}$; $r^2 = 0.9996$).

The response is linear between 27 and 43 °C, a suitable range for monitoring cell cultures [47]. The micrometric thickness of the sensitive spots has positive and negative consequences. On the one hand, the response time (the delay between the thermistor and the optode signals) of the temperature-sensitive film is shorter than 5 s. On the other, the thin sensor is no longer insensitive to O₂ (see Figure S5, Supplementary Materials). However, this interference is easily suppressed by measuring that species and temperature at the same time, something that can be readily performed in a multichannel instrument, like ours. Moreover, the interference of O₂ can be eliminated by covering the dyed PCA spot with commercial aluminum foil which, besides decreasing external light interference blocks permeation of gases without lowering the sensor sensitivity to temperature.

4. Conclusions

Molecular engineering of Ru(II) polypyridyl complexes allows for the design and manufacture of luminescent temperature sensors that outperform those described up to date based on standard Ru(II) indicator dyes for oxygen monitoring. In this way, a novel heteroleptic complex with two 1,10-phenanthroline and one 4-chloro-1,10-phenanthroline ligands embedded in poly(cyanoacrylate) provides optimum temperature response and photostability (at least) in the 0–50 °C range, using both emission intensity- or lifetime-based measurements with commercially-available instrumentation for optical O₂ sensing. Moreover, this polymeric material provides affordable, easily made, and reproducible sensitive elements with excellent optical quality that can be tailored to the sought application.

The applications of polymer-based luminescent temperature sensors doped with Ru(II) complexes are countless and not only restricted to those illustrated here, namely temperature monitoring of surface waters in combination with other Ru(II)-polypyridyl-based optodes (O₂, pH, CO₂, NH₃, Cu^{II}, etc.) [10] plus a multichannel field-deployable optoelectronic unit, and cell culture monitoring with lab-on-a-chip systems. Other uses where such polymeric optical sensors may provide a definitive advantage are currently being investigated, e.g., temperature monitoring in bioreactors, aerospace applications, and temperature measurements within cells and tissues (the latter upon encapsulation of the indicator dye in polymer nanocapsules).

Supplementary Materials: The following items are available online at <http://www.mdpi.com/2073-4360/10/3/234/s1>, Figure S1: Picture of the temperature-sensitive optical fiber tips, Figure S2: Drawings/pictures of the 3-layer chip, temperature-sensitive spots into Micronit's organ-on-a-chip device, and of the Fluidic Connect PRO chip holder with fluidic connections and optical fibers, Figure S3: Variation with temperature of the luminescence intensity from the dye-doped polymer monoliths, Figure S4: Response to O₂ of the [Ru(phen)₂(4-Clp)]/PCA temperature-sensitive optical fiber tip, Figure S5: Response to O₂ of the [Ru(phen)₂(4-Clp)]/PCA temperature-sensitive spots in the organ-on-a-chip device.

Acknowledgments: Nelia Bustamante thanks the Spanish MINECO for a doctoral grant (F.P.I. program). Guido Ielasi thanks the EU ITN "SAMOSS" Marie Curie Action (FP7-PEOPLE-2013-ITN, ID 607590) grant. The authors thank the Spanish MINECO and the European Union Fund for Regional Development (FEDER) for the CTQ2015-69278-C2-2-R grant. They also thank Rocío Cuervo for her assistance in preparing EHMA-MMA copolymer. Micronit Microtechnologies B.V. (Enschede, The Netherlands) is gratefully acknowledged for providing the organ-on-a-chip devices, holders, adaptors, and all ancillary materials required during Guido Ielasi secondment to the company, and Dr. Sandro Meucci for his help and guidance therein.

Author Contributions: Guillermo Orellana designed the indicator dyes, most of the experiments, and directed the work. Nelia Bustamante prepared the indicator dye, the dye-doped monoliths and carried out the characterization and optimization of the indicator dyes and luminescent sensor. Guido Ielasi performed part of the photophysical characterization, checked the cited literature, and carried out the work on chips. Maximino Bedoya build the luminescence phase-sensitive equipment. All the authors contributed to the writing of the manuscript.

Conflicts of Interest: The authors declare no conflict of interest.

References and Note

- Childs, P.R.N.; Greenwood, J.R.; Long, C.A. Review of temperature measurement. *Rev. Sci. Instrum.* **2000**, *71*, 2959–2979. [[CrossRef](#)]
- Wang, X.-D.; Wolfbeis, O.S.; Meier, R.J. Luminescent probes and sensors for temperature. *Chem. Soc. Rev.* **2013**, *42*, 7834–7869. [[CrossRef](#)] [[PubMed](#)]
- Vollmer, M.; Möllmann, K.-P. Basic properties of IR imaging systems. In *Infrared Thermal Imaging: Fundamentals, Research and Applications*, 2nd ed.; Vollmer, M., Möllmann, K.-P., Eds.; Wiley-VCH Verlag GmbH & Co. KGaA: Weinheim, Germany, 2017; ISBN 9783527693306.
- Thompson, R.B. Fluorescence-based fiber-optic sensors. In *Topics in Fluorescence Spectroscopy*; Lakowicz, J.R., Ed.; Springer: Boston, MA, USA, 2002; Volume 2, pp. 345–365, ISBN 9780306470585.
- Uchiyama, S.; Gota, C.; Tsuji, T.; Inada, N. Intracellular temperature measurements with fluorescent polymeric thermometers. *Chem. Commun.* **2017**, *53*, 10976–10992. [[CrossRef](#)] [[PubMed](#)]
- Lee, Y.E.; Kopelman, R. Nanoparticle PEBBLE sensors in live cells. *Methods Enzymol.* **2012**, *504*, 419–470. [[CrossRef](#)] [[PubMed](#)]
- Hoera, C.; Ohla, S.; Shu, Z.; Beckert, E.; Nagl, S.; Belder, D. An integrated microfluidic chip enabling control and spatially resolved monitoring of temperature in micro flow reactors. *Anal. Bioanal. Chem.* **2015**, *407*, 387–396. [[CrossRef](#)] [[PubMed](#)]
- Okabe, K.; Inada, N.; Gota, C.; Harada, Y.; Funatsu, T.; Uchiyama, S. Intracellular temperature mapping with a fluorescent polymeric thermometer and fluorescence lifetime imaging microscopy. *Nat. Commun.* **2012**, *3*, 705–713. [[CrossRef](#)] [[PubMed](#)]
- Borisov, S.M.; Wolfbeis, O.S. Temperature-sensitive europium(III) probes and their use for simultaneous luminescent sensing of temperature and oxygen. *Anal. Chem.* **2006**, *78*, 5094–5101. [[CrossRef](#)] [[PubMed](#)]
- Orellana, G.; García-Fresnadillo, D. Environmental and industrial optosensing with tailored luminescent Ru(II) polypyridyl complexes. In *Optical Sensors: Industrial Environmental and Diagnostic Applications*; Springer: Berlin/Heidelberg, Germany, 2004; pp. 309–357.
- Zhou, H.; Sharma, M.; Berezin, O.; Zuckerman, D.; Berezin, M.Y. Nanothermometry: From microscopy to thermal treatments. *ChemPhysChem* **2016**, *17*, 27–36. [[CrossRef](#)] [[PubMed](#)]
- Wang, X.-D.; Wolfbeis, O.S. Optical methods for sensing and imaging oxygen: Materials, spectroscopies and applications. *Chem. Soc. Rev.* **2014**, *43*, 3666–3761. [[CrossRef](#)] [[PubMed](#)]
- For instance, the Ocean Optics (USA) Foxy[®], Presens (Germany) Microx[®], Van Essen Instruments (The Netherlands) Diver[®], or PyroScience (Germany) FireStingO₂[®] fiber-optic oxygen monitors.
- Demas, J.N.; DeGraff, B.A. Design and applications of highly luminescent transition metal complexes. In *Topics in Fluorescence Spectroscopy*; Lakowicz, J.R., Ed.; Springer: Boston, MA, USA, 2002; Volume 4, ISBN 9780306470608.

15. Klimant, I.; Holst, G. Optical Temperature Sensors and Optical-Chemical Sensors with Optical Temperature Compensation. U.S. Patent 6,303,386, 24 May 2001.
16. Mills, A.; Tommons, C.; Bailey, R.T.; Tedford, M.C.; Crilly, P.J. Luminescence temperature sensing using poly(vinyl alcohol)-encapsulated Ru(bpy)₃²⁺ films. *Analyst* **2006**, *131*, 495–500. [[CrossRef](#)] [[PubMed](#)]
17. Miranda, M.; Levi, V.; Bossi, M.L.; Bruno, L.; Bordoni, A.V.; Reqazzoni, A.E.; Wolosiuk, A. Temperature response of luminescent tris(bipyridine)ruthenium(II)-doped silica nanoparticles. *J. Colloid Interface Sci.* **2013**, *392*, 96–101. [[CrossRef](#)] [[PubMed](#)]
18. Tsvirko, M.; Tkaczyk, S.; Kozak, M.; Kalota, B. Luminescent temperature sensor based on [Ru(bpy)₃]²⁺ incorporated into chitosan. *Funct. Mater.* **2013**, *20*, 127–132. [[CrossRef](#)]
19. Huang, C.-Y.; Huang, B.-H.; Cheng, F.-R.; Chen, S.-W.; Liou, T.-M. Experimental study of heat transfer enhancement with segmented flow in a microchannel by using molecule-based temperature sensors. *Int. J. Heat Mass Transf.* **2017**, *107*, 657–666. [[CrossRef](#)]
20. Koese, M.E.; Carroll, B.F.; Schanze, K.S. Preparation and spectroscopic properties of multiluminophore luminescent oxygen and temperature sensor films. *Langmuir* **2005**, *21*, 9121–9129. [[CrossRef](#)] [[PubMed](#)]
21. Tolosa, L.; Lam, H.; Kostov, Y.; Falk, S.M.; Rao, G. Luminescence Based Noninvasive Remote Parameter Sensor and Sensing Method. U.S. Patent US 9,560,974 B2, 7 February 2017.
22. Zhang, H.; Lei, B.; Dong, H.; Liu, Y.; Zheng, M.; Xiao, Y. Temperature and oxygen sensing properties of Ru(II) covalently-grafted sol-gel derived ormosil hybrid materials. *J. Nanosci. Nanotechnol.* **2016**, *16*, 4023–4028. [[CrossRef](#)] [[PubMed](#)]
23. Pfeiffer, S.A.; Nagl, S. On-chip photothermal analyte detection using integrated luminescent temperature sensors. *Anal. Chem.* **2017**, *89*, 9400–9406. [[CrossRef](#)] [[PubMed](#)]
24. Draxler, S. Temperature dependence of the photophysical properties of ruthenium diphenylphenanthroline in liquid and solid environments. *J. Phys. Chem. A* **1999**, *103*, 4719–4722. [[CrossRef](#)]
25. Klein, C.; Henne, U.; Constantini, M.; Beifuss, U.; Ondrus, V. Ruthenium Compound as a Temperature Probe in a Temperature-Sensitive Paint for Use at Low Temperatures [Ruthenium-Verbindung als Temperatursonde in einer Temperaturempfindlichen Farbe für den Einsatz bei Niedrigen Temperaturen]. Ger. Patent DE 102,015,104,585 B3, 8 September 2016.
26. García-Fresnadillo, D.; Georgiadou, Y.; Orellana, G.; Braun, A.M.; Oliveros, E. Singlet-oxygen (¹Δ_g) production by ruthenium(II) complexes containing polyazaheterocyclic ligands in methanol and in water. *Helv. Chim. Acta* **1996**, *79*, 1222–1238. [[CrossRef](#)]
27. Lumpkin, R.S.; Kober, E.M.; Worl, L.A.; Murtaza, Z.; Meyer, T.J. Metal-to-ligand charge-transfer (MLCT) photochemistry: Experimental evidence for the participation of a higher lying MLCT state in polypyridyl complexes of ruthenium(II) and osmium(II). *J. Phys. Chem.* **1990**, *94*, 239–243. [[CrossRef](#)]
28. Pourtois, G.; Beljonne, D.; Moucheron, C.; Schumm, S.; Kirsch-De Mesmaeker, A.; Lazzaroni, R.; Brédas, J.-L. Photophysical properties of ruthenium(II) polyazaaromatic compounds: A theoretical insight. *J. Am. Chem. Soc.* **2004**, *126*, 683–692. [[CrossRef](#)] [[PubMed](#)]
29. Sun, Q.; Mosquera-Vazquez, S.; Daku, L.M.; Guénée, L.; Goodwin, H.A.; Vauthey, E.; Hauser, A. Experimental evidence of ultrafast quenching of the ³MLCT luminescence in ruthenium(II) tris-bipyridyl complexes via a ³dd state. *J. Am. Chem. Soc.* **2013**, *135*, 13660–13663. [[CrossRef](#)] [[PubMed](#)]
30. Van Houten, J.; Watts, R.J. Temperature dependence of the photophysical and photochemical properties of the tris(2,2'-bipyridyl)ruthenium(II) ion in aqueous solution. *J. Am. Chem. Soc.* **1976**, *98*, 4853–4858. [[CrossRef](#)]
31. Seddon, E.A.; Seddon, K.R. *The Chemistry of Ruthenium*; Clark, R.J.H., Ed.; Elsevier: Amsterdam, The Netherlands, 1984; Volume 19, pp. 1228–1236, ISBN 9781483289908.
32. Rillema, D.P.; Allen, G.; Meyer, T.J.; Conrad, D. Redox properties of ruthenium(II) tris chelate complexes containing the ligands 2,2'-bipyrazine, 2,2'-bipyridine, and 2,2'-bipyrimidine. *Inorg. Chem.* **1983**, *22*, 1617–1622. [[CrossRef](#)]
33. Sullivan, B.P.; Salmon, D.J.; Meyer, T.J. Mixed phosphine 2,2'-bipyridine complexes of ruthenium. *Inorg. Chem.* **1978**, *17*, 3334–3341. [[CrossRef](#)]
34. Snyder, H.R.; Freier, H.E. Some substituted 1,10-phenanthrolines. *J. Am. Chem. Soc.* **1946**, *68*, 1320–1322. [[CrossRef](#)] [[PubMed](#)]
35. García-Fresnadillo, D. Molecular Engineering and Photochemistry of Ru(II) Luminescent Indicators for Oxygen, Detergents and Pesticides Optosensing. Ph.D. Thesis, Universidad Complutense de Madrid, Madrid, Spain, 1996.

36. Gutiérrez-Alonso, M.C. Luminescent DNA Probes and Photonucleases Based on Intercalating Viologens and Ru(II) Polypyridyls. Ph.D. Thesis, Universidad Complutense de Madrid, Madrid, Spain, 1996.
37. Villeras, J.; Ramband, M. Wittig-Horner reaction in heterogeneous media; 1. An easy synthesis of ethyl α -hydroxymethylacrylate and ethyl α -halomethylacrylates using formaldehyde in water. *Synthesis* **1982**, *11*, 924–926. [[CrossRef](#)]
38. Mielenz, K.D. Measurements of photoluminescence. In *Optical Radiation Measurements*; Grum, F., Bartleson, C.J., Eds.; Academic Press: New York, NY, USA, 1982; Volume 3, ISBN 9780123049032.
39. Suzuki, K.; Kobayashi, A.; Kaneko, S.; Takehira, K.; Yoshihara, T.; Ishida, H.; Shiina, Y.; Oishi, S.; Tobita, S. Reevaluation of absolute luminescence quantum yields of standard solutions using a spectrometer with an integrating sphere and a back-thinned CCD detector. *Phys. Chem. Chem. Phys.* **2009**, *11*, 9850–9860. [[CrossRef](#)] [[PubMed](#)]
40. Valeur, B.; Berberan-Santos, M.N. *Molecular Fluorescence. Principles and Applications*, 2nd ed.; Wiley-VCH Verlag & Co. KGaA: Weinheim, Germany, 2012; ISBN 9783527328376.
41. Lakowicz, J.R. *Principles of Fluorescence Spectroscopy*, 3rd ed.; Springer: New York, NY, USA, 2006; ISBN 9780387463124.
42. Sykora, M.; Kincaid, J.R. Synthetic manipulation of excited state decay pathways in a series of ruthenium(II) complexes containing bipyrazine and substituted bipyridine ligands. *Inorg. Chem.* **1995**, *34*, 5852–5856. [[CrossRef](#)]
43. Allen, G.H.; White, R.P.; Rillema, D.P.; Meyer, T.J. Synthetic control of excited-state properties. Tris-chelate complexes containing the ligands 2,2'-bipyrazine, 2,2'-bipyridine, and 2,2'-bipyrimidine. *J. Am. Chem. Soc.* **1984**, *106*, 2613–2620. [[CrossRef](#)]
44. Jacquet, L.; Kirsch-De Mesmaeker, A. Spectroelectrochemical characteristics and photophysics of a series of Ru(II) complexes with 1,4,5,8,9,12-hexaazatriphenylene: Effects of polycomplexation. *J. Chem. Soc. Faraday Trans.* **1992**, *88*, 2471–2480. [[CrossRef](#)]
45. Rillema, D.P.; Blanton, C.B.; Shaver, R.J.; Jackman, D.C.; Boldaji, M.; Bundi, S.; Worl, L.A.; Meyer, T.J. MLCT-dd energy gap in pyridyl-pyrimidine and bis(pyridine) complexes of ruthenium(II). *Inorg. Chem.* **1992**, *31*, 1600–1606. [[CrossRef](#)]
46. Orellana, G.; Cano-Raya, C.; López-Gejo, J.; Santos, A.R. Online Monitoring Sensors. In *Treatise on Water Science*; Wilderer, P., Ed.; Elsevier: Oxford, UK, 2011; Volume 3, pp. 221–262, ISBN 9780444531933.
47. Ozturk, S.; Hu, W.-S. *Cell Culture Technology for Pharmaceutical and Cell-Based Therapies*; CRC Press: Boca Raton, FL, USA, 2005.
48. Masterton, R.J.; Smales, C.M. The impact of process temperature on mammalian cell lines and the implications for the production of recombinant proteins in CHO cells. *Pharm. Bioprocess.* **2014**, *2*, 49–61. [[CrossRef](#)]
49. Maruszewski, K.; Strommen, D.P.; Kincaid, J.R. Zeolite-entrapped ruthenium(II) complexes with bipyridine and related ligands. Elimination of ligand-field-state deactivation and increase in 3 MLCT state lifetimes. *J. Am. Chem. Soc.* **1993**, *115*, 8345–8350. [[CrossRef](#)]
50. Sen, R.; Koner, S.; Bhattacharjee, A.; Kusz, J.; Miyashita, Y.; Okamoto, K. Entrapment of $[\text{Ru}(\text{bpy})_3]^{2+}$ in the anionic metal-organic framework: Novel photoluminescence behavior exhibiting dual emission at room temperature. *Dalton Trans.* **2011**, *40*, 6952–6960. [[CrossRef](#)] [[PubMed](#)]
51. Chen, R.; Zhang, J.; Chelora, J.; Xiong, Y.; Kershaw, S.V.; Li, K.F.; Lo, P.-K.; Cheah, K.W.; Rogach, A.L.; Zapien, J.A.; et al. Ruthenium(II) complex incorporated UiO-67 metal-organic framework nanoparticles for enhanced two-photon fluorescence imaging and photodynamic cancer therapy. *ACS Appl. Mater. Interfaces* **2017**, *9*, 5699–5708. [[CrossRef](#)] [[PubMed](#)]
52. López-Gejo, J.; Haigh, D.; Orellana, G. Relationship between the microscopic and macroscopic world in optical oxygen sensing: A luminescence lifetime microscopy study. *Langmuir* **2010**, *26*, 2144–2150. [[CrossRef](#)] [[PubMed](#)]

